Journal of The Electrochemical Society, **157** (3) H361-H370 (2010)
0013-4651/2010/157(3)/H361/10/$28.00 © The Electrochemical Society

Removal of Ion-Implanted Photoresists Using Atomic Hydrogen

Masashi Yamamoto,[a,z] Takeshi Maruoka,[a] Yousuke Goto,[a] Akihiko Kono,[a] Hideo Horibe,[a] Mune-aki Sakamoto,[a] Eiji Kusano,[a] Hirofumi Seki,[b] and Seiichi Tagawa[c]

[a]*Kanazawa Institute of Technology, Hakusan, Ishikawa 924-0838, Japan*
[b]*Toray Research Center, Incorporated, Otsu, Shiga 520-8567, Japan*
[c]*Osaka University, Ibaraki, Osaka 567-0047, Japan*

In this paper, we investigated the removal characteristic of positive-tone novolak photoresists into which B, P, and As ions were implanted with doses of 5×10^{12}–5×10^{15} atoms/cm^2 at an acceleration energy of 70 keV using atomic hydrogen, and the hardening mechanisms for the photoresists. All of the ion-implanted photoresists with doses up to 5×10^{15} atoms/cm^2 were removed without regard for ion species. The removal rates of the photoresists decreased with increasing ion-implantation dose due to hardening of the photoresist surfaces with implantation. The thickness of the surface-hardened layer of the photoresists decreased in the order of B → P → As, and the removal rate increased with decreasing thickness. The energy supplied from the ions to the photoresist concentrated on the surface side in the order of B → P → As, and the impact of the heavier ion on the photoresist was greater than that of the lighter ion. We deduced that the photoresists exhibited carbonization and cross-linkage attributable to the decrease in OH, CH, and O 1s and the increase in C═C, C 1s, and π-conjugated systems.
 [DOI: 10.1149/1.3288697]

Manuscript submitted October 12, 2009; revised manuscript received November 27, 2009. Published January 28, 2010.

In semiconductor manufacturing, ion implantation is one of the most important processes in fabricating p-/n-semiconductor devices. In this process, a group of 13 or 15 elements (e.g., B, P, and As ions) are irradiated over the entire area of a substrate on which photoresist patterns have been fabricated. The photoresist functions as a mask for the substrate, so the ions are also implanted into the photoresist. Once the photoresist has been denaturalized by implanted ions,[1-7] it is difficult to remove.[1,4,8-12] Although the removal of the photoresist is troublesome at present, the photoresist is actually removed by combining oxygen plasma ashing and chemicals (e.g., a sulfuric acid–hydrogen peroxide mixture and an ammonia–hydrogen peroxide mixture). However, these methods have certain problems, such as unwanted oxidation of the substrates and metal interconnects and etching, as well as the handling of chemicals, the disposal of waste chemicals, and cleaning process. To overcome these problems, we have previously investigated ion-implanted photoresist removal by oxidation degradation using wet ozone.[9,12] However, none of the photoresists with doses exceeding 5×10^{14} atoms/cm^2 were removed by wet ozone, except for a B-ion-implanted photoresist with a dose of 5×10^{14} atoms/cm^2.[9,12] In this study, we examined the removal characteristic of an ion-implanted photoresist with high doses using atomic hydrogen, which has excellent reduction ability, and the hardening mechanism for a photoresist by ion implantation.

Atomic hydrogen is generated by decomposing a hydrogen molecule by contact with a hot-wire tungsten catalyst.[13,14] Some findings on photoresist removal using atomic hydrogen generated with hot-wire tungsten catalysts have already been reported.[11,15-18] The photoresist is decomposed into $-C_xH_y$ and –OH compounds by atomic hydrogen.[19] It is also believed that implanted ions are decomposed into volatile gases (e.g., B_2H_6, PH_3, and AsH_3). This catalytic decomposition method is plasma-free, thus avoiding plasma damage to devices. Oxidation of semiconductor substrates and metal interconnects is not expected. Additionally, atomic hydrogen generated on heated metal catalysts has been used for semiconductor engineering, such as in passivation,[20] dangling-bond termination,[21] crystallization of amorphous Si,[22] and surface cleaning.[23-25]

In this paper, we investigated the removal characteristic of positive-tone novolak photoresists implanted with B, P, and As ions at an implantation dose of 5×10^{12}–5×10^{15} atoms/cm^2 at 70 keV of acceleration energy using atomic hydrogen, and the hardening mechanism for the photoresists. In general, the photoresist subsurface layer, through which the ions passed, may be carbonized.[1-7] We evaluated the hardness depth profiles of the photoresists using nanoindentation,[26-30] simulated the behavior of ions implanted into the photoresists using Stopping Range of Ions in Materials (SRIM),[31] and investigated the hardening mechanism for the photoresists using optical spectroscopy [Fourier transform IR (FTIR), Raman, and UV] and X-ray photoelectron spectroscopy (XPS).

[z] E-mail: m-yamamoto@venus.kanazawa-it.ac.jp

Experimental

Ion-implanted photoresist preparation.— A positive-tone novolak photoresist (AZ6112; AZ-Electronic Materials) was used for this study. It was spin-coated onto a Si wafer using a spin coater (ACT-300A; Active) at 2000 rpm for 20 s and then prebaked at 100°C for 1 min on a hot plate (PMC 720 series; Dataplate). The photoresist film thickness (0.9 ± 0.1 μm) was measured using a stylus-type surface-profile measurement instrument (DekTak 6M; ULVAC). The B, P, and As ions were implanted into the photoresists with doses of 5×10^{12}–5×10^{15} atoms/cm^2 and an acceleration energy of 70 keV without cooling. Table I lists the film thickness, ion current, and implantation time for each ion-implanted photoresist. During implantation, the pressure inside the chamber was 10^{-6} Pa. The substrate temperature before implantation was 23°C (room temperature); however, the temperature was not monitored and may have risen to a few hundred °C during implantation.[32]

Ion-implanted photoresist removal using atomic hydrogen.— Figure 1 presents a schematic diagram of the experiment apparatus. Table II lists the experiment conditions for photoresist removal. Mixed hydrogen–nitrogen gas (H_2:N_2 = 10:90 vol %) flowed from the center nozzle into a fused silica chamber. The hydrogen gas flow rate was fixed at 30 sccm using a mass-flow controller. The hydrogen gas pressure was 2.13 Pa. Nitrogen gas was used to dilute the concentration of the hydrogen gas and thus avoid an explosion. The density of atomic nitrogen generated by a hot catalyst was very low (less than 10^{10} cm^{-3})[33] compared with that of atomic hydrogen (10^{14} cm^{-3})[34] when a tungsten catalyst temperature (T_W) was 2770 K. Therefore, atomic nitrogen has little effect on photoresist removal.

A resistively heated tungsten wire (99.95%, 0.7 mm in diameter, and 500 mm in length; Nilaco Corp.) was used as a hot catalyst to generate atomic hydrogen. The 40 mm long, 10 mm diameter catalyst was coiled into a helix with five turns. The distance between the catalyst and the substrate (D_{CS}) was set at 100 mm. The catalyst was heated to 2420°C (T_W) using a dc power supply. T_W was measured using a dual-wavelength (0.8 and 1.05 μm) IR radiation thermometer (ISR12-L0; Impac Electronic GmbH). The initial substrate temperature ($T_{ini\text{-}subst}$) was set at room temperature (25°C). The sub-

Table I. Film thickness, ion current, and implantation time for each ion-implanted photoresist.

Ion species (at 70 keV)	Implantation dose (atom/cm^2)	Film thickness (μm)	Ion current (μA)	Implantation time (s)
—	Nonimplantation	0.9 ± 0.1	—	—
B	5×10^{12}	0.84	4.5	33
B	5×10^{13}	0.85	29.3	51
B	5×10^{14}	0.85	46.9	320
B	5×10^{15}	0.73	61.6	2410
P	5×10^{12}	0.99	4.9	38
P	5×10^{13}	0.99	31.0	48
P	5×10^{14}	0.95	52.8	282
P	5×10^{15}	0.93	63.5	2325
As	5×10^{12}	0.98	5.0	30
As	5×10^{13}	0.93	30.9	49
As	5×10^{14}	0.86	53.6	278
As	5×10^{15}	0.78	61.5	2435

strate temperature was monitored with a Chromel–Alumel thermocouple during atomic hydrogen irradiation. Thermolabels (Nichiyu Giken Kogyo Co., Ltd.) were also used to check the temperature measured with the thermocouple.

In this experiment, we measured the change in the B-, P-, and As-ion-implanted photoresist film thickness with respect to the atomic hydrogen irradiation time. If D_{CS} is shortened to 20 mm, it is possible to relatively quickly remove ion-implanted photoresists with higher doses.[11] However, during atomic hydrogen irradiation, the substrate was heated up to a few hundred °C, and "popping" occurred. Popping is a phenomenon in which a surface-hardened layer (SHL) pops by outgassing (e.g., vaporized solvent generated at an underlayer of the photoresist by heating an ion-implanted photoresist).[10] The solvent remained in the underlayer because the underlayer was not influenced by the ion implantation. If popping were to occur on the photoresists, it would be difficult to measure the film thickness because of the bumpy surface of the photoresist. We extended D_{CS} to 100 mm not to generate outgassing by suppressing substrate heating. Besides, to avoid popping by increasing the paths for outgassing, we scratched the surface of the photoresists in a gridlike pattern at intervals of 500 μm before atomic-hydrogen irradiation.

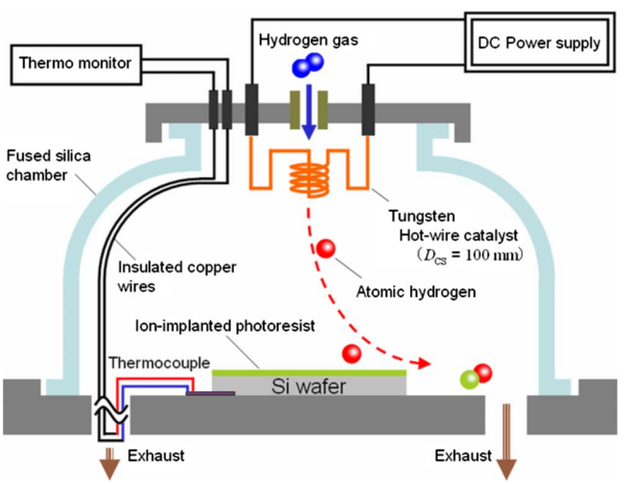

Figure 1. (Color online) Schematic diagram of the experiment apparatus. The distance between the tungsten catalyst and the photoresist substrate (D_{CS}) was 100 mm, and the catalyst temperature (T_W) was 2420°C.

Table II. Experiment conditions for photoresist removal by atomic hydrogen.

Parameter	Value
Substrate temperature ($T_{ini\text{-}subst}$)	Room temperature (25°C)
Hot catalyst temperature (T_W)	2420°C
H_2/N_2 (10/90 vol %) gas inflow rate	300 sccm
Hydrogen gas inflow rate	30 sccm
Total pressure in chamber	21.3 Pa
Hydrogen pressure in chamber	2.13 Pa
Distance between catalyst and substrate (D_{CS})	100 mm

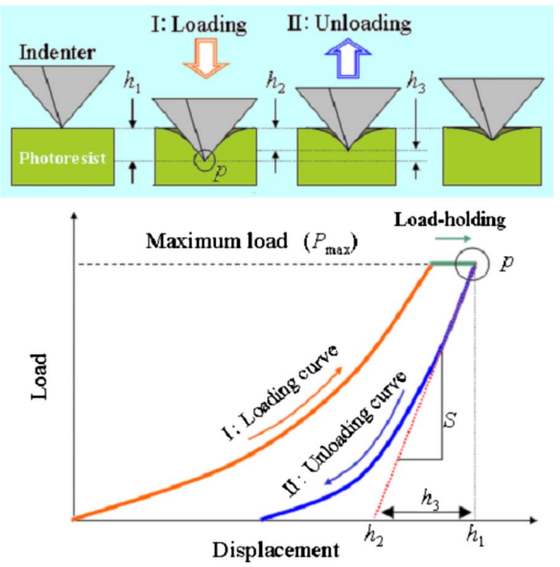

Figure 2. (Color online) Schematic diagram of the nanoindentation experiment apparatus.

Evaluation of Young's modulus of ion-implanted photoresist using nanoindentation.— Figure 2 presents a schematic diagram of the hardness evaluation for each ion-implanted photoresist by nanoindentation (ENT-1040; Elionix). Using nanoindentation, we obtained a loading–unloading curve that consisted of a loading curve, a load holding, and an unloading curve. Here, as indicated in Fig. 2, P_{max} is the maximum load, h_1 is the indentation depth (point p), S is the slope of the tangent to the unloading curve from p, and h_2 is the depth at which the tangent intersects the x-axis. Table III lists the experiment conditions for nanoindentation. We examined Young's modulus at various depths (h_1) by changing P_{max} from 1 to 360 mgf. The loading–unloading rate was set at 0.004 mgf/ms (lower limit) for a load of 1 to 8 mgf, and at P_{max}/2000 mgf/ms for a load of more than 8 mgf. The load-holding time between loading and unloading was 2 s. A Berkovich-type diamond indenter with an apex angle of 115° was used for this work. We evaluated the reduced

Table III. Experiment conditions for evaluating ion-implanted photoresist hardness by nanoindentation.

Parameter	Value
Maximum load (P_{max})	1–320 mgf
Loading–unloading rate (1 to 8 mgf)	0.004 mgf/ms
Loading–unloading rate (more than 8 mgf)	(P_{max}/2000) mgf/ms
Load-holding time	2 s
Indenter material	Diamond
Indenter type	Berkovich (Apex angle 115°)

modulus (E_R) for each ion-implanted photoresist using S obtained from the unloading curves at various loads (Eq. 1)

$$E_R = \frac{\sqrt{\pi}}{2}\frac{1}{\sqrt{A}}S \quad [1]$$

Here, A, defined in Eq. 2, is the projected area of contact at peak load and is a function of h_2. $f(h_2)$ represents the deviation from the geometry due to blunting at the tip

$$A = 24.5h_2^2 + f(h_2) \quad [2]$$

Parameter h_2 is related to h_1 and h_3, as shown in the equations below and as indicated in Fig. 2

$$h_1 = h_2 + h_3$$

$$h_3 = \varepsilon\frac{P_{max}}{S} \quad [3]$$

h_1, P_{max}, and S can be measured by nanoindentation. ε is a factor attributable to the indenter configuration and was 0.75 for the Berkovich-type indenter. E_R was obtained by substituting Eq. 2 and 3 into Eq. 1. Eventually, Young's modulus (E_S) of the photoresists was calculated using Eq. 4

$$E_S = \frac{1-\mu_S^2}{\frac{1}{E_R} - \frac{1-\mu_I^2}{E_I}} \quad [4]$$

where μ_S is Poisson's ratio for the photoresists and is about 0.3 for polymers.[35-37] E_I and μ_I are Young's modulus and Poisson's ratio for the indenter and are 1140 GPa and 0.07, respectively. We evaluated E_S of the ion-implanted photoresist, normalized by the E_S of the nonimplanted photoresist (E_S of AZ6112), and defined it as the normalized E_S. The normalized E_S was obtained by dividing the E_S of the ion-implanted photoresist by the E_S of AZ6112.

Investigation of ion-implanted photoresist hardening mechanism.— Ion-implanted photoresists would be denaturalized by the energy supplied from implanted ions to the photoresist during the interaction between the photoresist and the ions.[1-7] Using SRIM, we calculated the distributions of the ions implanted into the photoresists and the energy supplied from the ions to the photoresist (i.e., to the electrons and to elements such as C, O, and H, which are components of the photoresists). We used poly(methyl methacrylate) (PMMA) as the photoresist in SRIM because it was complicated to incorporate the effect of the resonance stability of benzene rings in novolak photoresists into the calculations.

We examined the change in molecular vibration in photoresists induced by ion implantation by using FTIR (7000FTIR with Ge prism ATR; Varian) and Raman spectroscopy (Ramanar T-64000; Jobin Yvon). FTIR spectra were measured over the wavenumber range of 670–4000 cm^{-1} with a resolution of 4 cm^{-1}. Raman spectra were measured over the wavenumber range of 600–2000 cm^{-1} using an Ar^+ laser (irradiation power 1 mW, wavelength 514.5 nm, and beam diameter 1 μm). We used a grating with 600 gr/mm, and the slit width was set to 100 μm. A 1024-channel charge-coupled device was used as a Raman detector.

We also examined the changes in a π-conjugated system attributable to the π–π^* absorption in photoresists by ion implantation using a UV spectrometer (UV-2450; Shimadzu). The π–π^* absorption was measured over the wavelengths of 190–280 nm with a resolution of 0.5 nm, using an integrating sphere (ISR-22000; Shimadzu, reflective mode) with an incident angle of 8°.

We performed surface-element analyses of the ion-implanted photoresists using an X-ray photoelectron spectroscope (ESCA-3400; Shimadzu). We etched 3–5 nm of the photoresist surfaces using Ar ions for 1 min before the XPS analysis because CO_2, O_2, N_2, and H_2O adsorbed on the photoresist surfaces exposed to air would adversely affect the XPS analysis. The acceleration voltage, beam current, and pressure for Ar-ion etching were 1 kV, 10 mA, and 5×10^{-4} Pa, respectively. The XPS analysis was performed with Mg Kα radiation. The Mg Kα X-ray source was operated at 10 kV and 10 mA. The base pressure of the XPS system was below 10^{-6} Pa. The XPS scan range was 1000–0 eV in 0.2 eV steps.

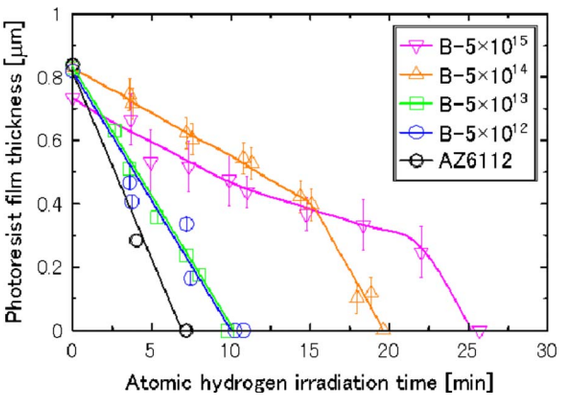

Figure 3. (Color online) Dependence of the B-ion-implanted photoresist film thickness on the atomic-hydrogen irradiation time. AZ6112 is a positive-tone novolak photoresist without ion implantation. The B-ion-implantation doses were 5×10^{12}–5×10^{15} atoms/cm^2, and the B-ion acceleration energy was 70 keV.

Results and Discussion

Characteristics of ion-implanted photoresist removal by atomic hydrogen.— Figure 3 depicts the change in B-ion-implanted photoresist film thickness with respect to the atomic-hydrogen irradiation time at various implantation doses. The film thickness of photoresists with B-ion-implantation doses of 5×10^{12} and 5×10^{13} atoms/cm^2 decreased in direct proportion to the atomic-hydrogen irradiation time, as with a nonimplanted photoresist (AZ6112). The removal rate (v_{rmv}) of the photoresist with doses of both 5×10^{12} and 5×10^{13} atoms/cm^2 was 0.083 μm/min. For photoresists with doses of more than 5×10^{14} atoms/cm^2, the layer in which the film thickness decreased a little with respect to the irradiation time was observed on the surface side. The subsurface layer was presumably an SHL. The thickness of the SHL [t(SHL)] of the photoresist with a dose of 5×10^{14} atoms/cm^2 was 0.43 ± 0.07 μm, and that with a dose of 5×10^{15} atoms/cm^2 was 0.43 ± 0.08 μm. The removal rates of the SHL [v_{rmv}(SHL)] were calculated as the change in the t(SHL) with respect to the irradiation time. v_{rmv}(SHL) with a dose of 5×10^{14} atoms/cm^2 was 0.029 ± 0.005 μm/min, and that with a dose of 5×10^{15} atoms/cm^2 was 0.020 ± 0.004 μm/min. However, after the SHL was removed, the photoresists were removed like AZ6112. Hence, the layer under the SHL was presumably a nonimplanted layer (NIL). The thickness of the NIL [t(NIL)] of the photoresist with a dose of 5×10^{14} atoms/cm^2 was 0.42 ± 0.07 μm, and that with a dose of 5×10^{15} atoms/cm^2 was 0.30 ± 0.08 μm. The removal rates of the NIL [v_{rmv}(NIL)] of the photoresists were also calculated as the change in the t(NIL) with respect to the irradiation time, as with v_{rmv}(SHL). v_{rmv}(NIL) with a dose of 5×10^{14} atoms/cm^2 was 0.089 ± 0.014 μm/min, and that with a dose of 5×10^{15} atoms/cm^2 was 0.088 ± 0.023 μm/min. v_{rmv} of the photoresist with a dose of 5×10^{14} atoms/cm^2 was 0.043 μm/min, and that with a dose of 5×10^{15} atoms/cm^2 was 0.029 μm/min. v_{rmv} and v_{rmv}(SHL) decreased with increasing implantation doses.

Figure 4 depicts the change in P-ion-implanted photoresist film thickness with respect to the atomic-hydrogen irradiation time at various implantation doses. The film thickness of photoresists with P-ion-implantation doses of 5×10^{12} and 5×10^{13} atoms/cm^2 de-

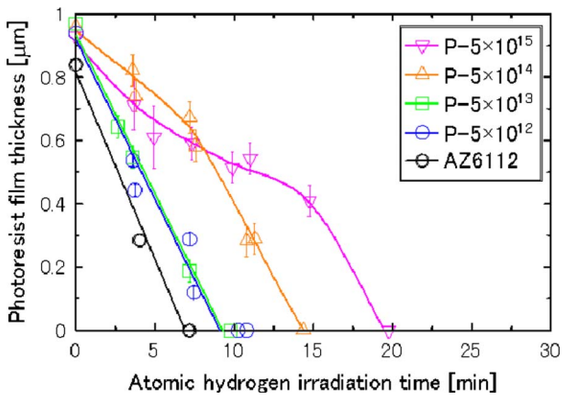

Figure 4. (Color online) Dependence of the P-ion-implanted photoresist film thickness on the atomic-hydrogen irradiation time. AZ6112 is a positive-tone novolak photoresist without ion implantation. The P-ion-implantation doses were 5×10^{12}–5×10^{15} atoms/cm^2, and the P-ion acceleration energy was 70 keV.

creased in direct proportion to the irradiation time, as with AZ6112. v_{rmv} of the photoresist with doses of both 5×10^{12} and 5×10^{13} atoms/cm^2 was 0.10 μm/min. For doses of more than 5×10^{14} atoms/cm^2, the film thickness on the surface side decreased

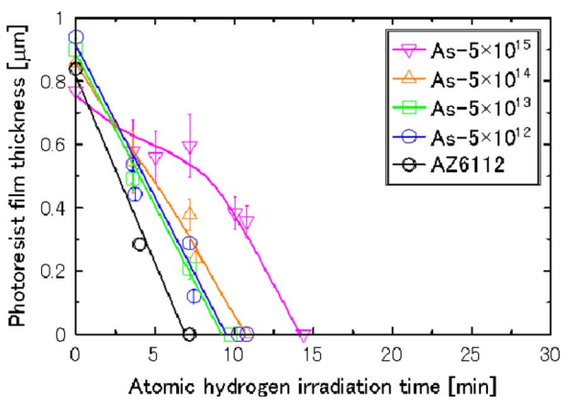

Figure 5. (Color online) Dependence of the As-ion-implanted photoresist film thickness on the atomic-hydrogen irradiation time. AZ6112 is a positive-tone novolak photoresist without ion implantation. The As-ion-implantation doses were 5×10^{12}–5×10^{15} atoms/cm^2, and the As-ion acceleration energy was 70 keV.

little with respect to the irradiation time, as with B-ion-implanted photoresist with the same dose. t(SHL) of the photoresist with a dose of 5×10^{14} atoms/cm^2 was 0.31 ± 0.07 μm, and that with a dose of 5×10^{15} atoms/cm^2 was 0.52 ± 0.06 μm. v_{rmv}(SHL) with a dose of 5×10^{14} atoms/cm^2 was 0.043 ± 0.009 μm/min, and that with a dose of 5×10^{15} atoms/cm^2 was 0.035 ± 0.004 μm/min. Also, after the SHL was removed, the photoresists were removed like AZ6112. t(NIL) of the photoresist with a dose of 5×10^{14} atoms/cm^2 was 0.64 ± 0.07 μm, and that with a dose of 5×10^{15} atoms/cm^2 was 0.41 ± 0.06 μm. v_{rmv}(NIL) with a dose of 5×10^{14} atoms/cm^2 was 0.090 ± 0.010 μm/min, and that with a dose of 5×10^{15} atoms/cm^2 was 0.087 ± 0.013 μm/min. v_{rmv} of the photoresist with a dose of 5×10^{14} atoms/cm^2 was 0.066 μm/min, and that with a dose of 5×10^{15} atoms/cm^2 was 0.049 μm/min. v_{rmv} and v_{rmv}(SHL) decreased with increasing implantation doses like B-ion-implanted photoresists.

Figure 5 depicts the change in As-ion-implanted photoresist film thickness with respect to the atomic-hydrogen irradiation time at various implantation doses. The film thickness of photoresists with As-ion-implantation doses of 5×10^{12} and 5×10^{13} atoms/cm^2 decreased in direct proportion to the irradiation time, as with AZ6112. v_{rmv} of the photoresist with doses of both 5×10^{12} and 5×10^{13} atoms/cm^2 was 0.10 μm/min. Even the photoresist with a dose of 5×10^{14} atoms/cm^2 was also removed, like the photoresists with doses of 5×10^{12} and 5×10^{13} atoms/cm^2. v_{rmv} of the photoresist with a dose of 5×10^{14} atoms/cm^2 was 0.081 μm/min. For the photoresists with a dose of 5×10^{15} atoms/cm^2, the film thickness on the surface side decreased little with respect to the irradiation time as with the B- and P-ion-implanted photoresists with the same dose. t(SHL) and v_{rmv}(SHL) of the photoresist with a dose of 5×10^{15} atoms/cm^2 were 0.24 ± 0.07 μm and 0.028 ± 0.009 μm/min, respectively. After the SHL was removed, the photoresists were removed like AZ6112. t(NIL) and v_{rmv}(NIL) of the photoresist with a dose of 5×10^{15} atoms/cm^2 were 0.54 ± 0.07 μm and 0.096±0.013 μm/min, respectively. v_{rmv} with a dose of 5×10^{15} atoms/cm^2 was 0.055 μm/min. v_{rmv} and v_{rmv}(SHL) decreased with increasing implantation dose like the B- and P-ion-implanted photoresists.

Consequently, Table IV lists the t(SHL), v_{rmv}(SHL), t(NIL), v_{rmv}(NIL), and v_{rmv} for each ion-implanted photoresist. It was possible to remove each ion-implanted photoresist with an implantation dose below 5×10^{13} atoms/cm^2, like AZ6112, using atomic hydrogen. The removal rates for these photoresists were almost the same. The photoresist would slightly denaturalize by ion implantation with these doses. For the photoresists with a dose of 5×10^{14} atoms/cm^2, the SHL was observed in the surface side, and

Table IV. Thickness of SHL [t(SHL)], removal rate of SHL [v_{rmv}(SHL)], thickness of NIL [t(NIL)], v_{rmv}(NIL), and v_{rmv} for each ion-implanted photoresist obtained by Fig. 3-5.

Ion species (at 70 keV)	Implantation dose (atom/cm^2)	t(SHL) (μm)	v_{rmv}(SHL) (μm/min)	t(NIL) (μm)	v_{rmv}(NIL) (μm/min)	v_{rmv} (μm/min)
—	Nonimplantation	—	—	0.84	0.12	0.12
B	5×10^{12}	—	—	0.84	0.083	0.083
B	5×10^{13}	—	—	0.85	0.083	0.083
B	5×10^{14}	0.43 ± 0.07	0.029 ± 0.005	0.42 ± 0.07	0.089 ± 0.014	0.043
B	5×10^{15}	0.43 ± 0.08	0.020 ± 0.004	0.30 ± 0.08	0.088 ± 0.023	0.029
P	5×10^{12}	—	—	0.99	0.10	0.10
P	5×10^{13}	—	—	0.99	0.10	0.10
P	5×10^{14}	0.31 ± 0.07	0.043 ± 0.009	0.64 ± 0.07	0.090 ± 0.010	0.066
P	5×10^{15}	0.52 ± 0.06	0.035 ± 0.004	0.41 ± 0.06	0.087 ± 0.013	0.049
As	5×10^{12}	—	—	0.98	0.10	0.10
As	5×10^{13}	—	—	0.93	0.10	0.10
As	5×10^{14}	—	—	0.86	0.081	0.081
As	5×10^{15}	0.24 ± 0.07	0.028 ± 0.009	0.54 ± 0.07	0.096 ± 0.013	0.055

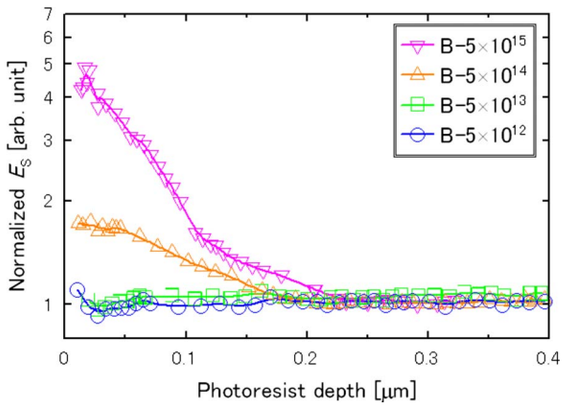

Figure 6. (Color online) Depth profiles for normalized Young's modulus (E_S) of B-ion-implanted photoresists. The normalized E_S value was obtained by dividing E_S of the ion-implanted photoresist by E_S of AZ6112, which was a positive-tone novolak photoresist without ion implantation. The B-ion-implantation doses were 5×10^{12}–5×10^{15} atoms/cm^2, and the B-ion acceleration energy was 70 keV.

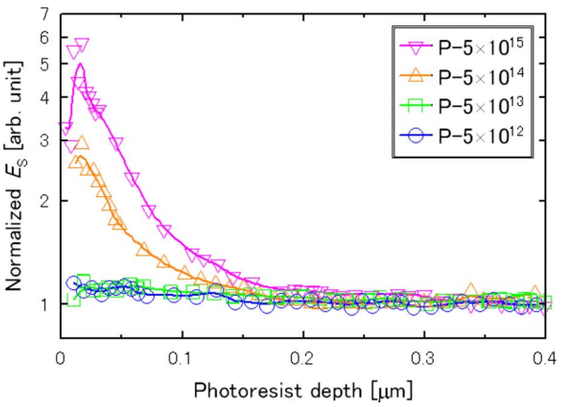

Figure 7. (Color online) Depth profiles for the normalized Young's modulus (E_S) of the P-ion-implanted photoresists. The normalized E_S value was obtained by dividing E_S of ion-implanted photoresist by E_S of AZ6112, which was a positive-tone novolak photoresist without ion implantation. The P-ion-implantation doses were 5×10^{12}–5×10^{15} atoms/cm^2, and the P-ion acceleration energy was 70 keV.

the v_{rmv}(SHL) was less than half of v_{rmv}(NIL). However, the effect of the SHL on the removal rate was hardly observed for the As-ion-implanted photoresist. After the SHL was removed, the photoresists were removed like AZ6112 because the layer under the SHL is not influenced by the implantation. For each ion-implanted photoresist, the v_{rmv}(SHL) and v_{rmv} with a dose of 5×10^{15} atoms/cm^2 were less than those with a dose of 5×10^{14} atoms/cm^2 because photoresists with doses exceeding 5×10^{14} atoms/cm^2 should harden with increasing ion implantation doses. v_{rmv} decreased with increasing implantation doses; it was more difficult to remove the photoresist with a higher dose. In one removal using wet ozone that we reported previously,[12] it was impossible to remove the ion-implanted photoresist with doses exceeding 5×10^{14} atoms/cm^2 except for a B-ion-implanted photoresist with a dose of 5×10^{14} atoms/cm^2. In contrast, we were able to remove high dose ion-implanted photoresists by using atomic hydrogen regardless of the ion species. However, v_{rmv} of the B-ion-implanted photoresist was the lowest, and v_{rmv} increased in the order of B → P → As. In reduction decomposition by atomic hydrogen, v_{rmv} of the photoresist implanted with lighter ions was lower, in contrast to oxidation decomposition by ozone.[9,10,12] If an implanted ion is lighter, the SHL may be widely formed but is relatively soft because the ions probably penetrate deep in the photoresist. However, if an implanted ion is heavier, the SHL may be locally formed on the photoresist surface but is relatively hard because the ions probably concentrate on the surface. In the photoresist removal using atomic hydrogen, as indicated in Fig. 3-5, not only the hardness of the SHL but also the t(SHL) would influence the removal characteristics. Hence, v_{rmv} is fast if the SHL is thin even if hard, whereas v_{rmv} is slow if the layer is thick even if more or less soft. Differences in the removal characteristics using atomic hydrogen attributable to ion species and implantation doses may be caused by the hardness and thickness of the SHL of the ion-implanted photoresists. Next, we evaluate the hardness depth profiles of the photoresists using nanoindentation.

Hardness of the ion-implanted photoresist.— Figure 6 plots the depth profiles for the normalized Young's modulus (normalized E_S) of the B-ion-implanted photoresists measured by nanoindentation. The normalized E_S was obtained by dividing the E_S of the ion-implanted photoresist by the E_S of a nonimplanted photoresist (AZ6112). Photoresists with doses below 5×10^{13} atoms/cm^2 had almost the same hardness as AZ6112. The E_S of photoresists with doses exceeding 5×10^{14} atoms/cm^2 increased with increasing ion-implantation dose. For B-ion-implanted photoresists with doses exceeding 5×10^{14} atoms/cm^2, the SHL was observed from the surface to a depth of about 0.20 μm. The E_S peak for a photoresist with a dose of 5×10^{14} atoms/cm^2 was 1.7, and that with a dose 5×10^{15} atoms/cm^2 was 4.9.

Figure 7 plots depth profiles of normalized E_S of the P-ion-implanted photoresists. Photoresists with doses below 5×10^{13} atoms/cm^2 had almost the same hardness as AZ6112 like B-ion-implanted photoresists. Also, the E_S of photoresists with doses exceeding 5×10^{14} atoms/cm^2 increased with increasing ion-implantation dose. For P-ion-implanted photoresists with doses exceeding 5×10^{14} atoms/cm^2, the SHL was observed from the surface to a depth of about 0.15 μm. The SHL shifted toward the surface of the photoresists compared with B-ion-implanted photoresists. The E_S peak for a photoresist with a dose of 5×10^{14} atoms/cm^2 was 3, and that for one with a dose of 5×10^{15} atoms/cm^2 was 5.7.

Figure 8 depicts the depth profiles of normalized E_S of the As-ion-implanted photoresists. Photoresists with a dose of 5×10^{12} atoms/cm^2 had almost the same hardness as AZ6112 like the B- and P-ion-implanted photoresists. For a photoresist with a dose of 5×10^{13} atoms/cm^2, a slight SHL was observed, unlike the B- and P-ion-implanted photoresists with the same dose. For the

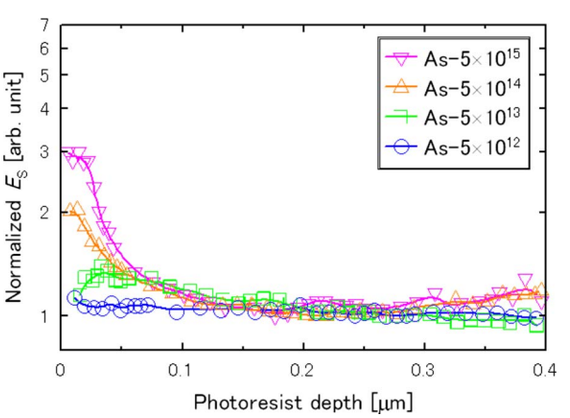

Figure 8. (Color online) Depth profiles for the normalized Young's modulus (E_S) of As-ion-implanted photoresists. The normalized E_S value was obtained by dividing E_S of the ion-implanted photoresist by E_S of AZ6112, which was a positive-tone novolak photoresist without ion implantation. The As-ion-implantation doses were 5×10^{12}–5×10^{15} atoms/cm^2, and the As-ion acceleration energy was 70 keV.

Table V. The thickness of SHL [t(SHL)] and normalized E_S peak for each ion-implanted photoresist obtained by Fig. 6-8.

Ion species (at 70 keV)	Implantation dose (atom/cm^2)	t(SHL) (μm)	Normalized E_S peak (arb. unit)
—	Nonimplantation	—	1
B	5×10^{12}	—	1
B	5×10^{13}	—	1
B	5×10^{14}	0.18	1.7
B	5×10^{15}	0.22	4.9
P	5×10^{12}	—	1
P	5×10^{13}	—	1
P	5×10^{14}	0.15	3.0
P	5×10^{15}	0.17	5.7
As	5×10^{12}	—	1
As	5×10^{13}	0.13	1.3
As	5×10^{14}	0.11	2.0
As	5×10^{15}	0.12	3.0

As-ion-implanted photoresists, the E_S of photoresists with doses exceeding 5×10^{13} atoms/cm^2 increased with increasing ion-implantation doses. The SHL was observed from the surface to a depth of about 0.10 μm. The SHL shifted toward the surface of the photoresists compared with the P-ion-implanted photoresists. The E_S peak of a photoresist with a dose of 5×10^{13} atoms/cm^2 was 1.3, that for one with a dose of 5×10^{14} atoms/cm^2 was 2, and that for one with a dose of 5×10^{15} atoms/cm^2 was 3.

Consequently, Table V lists the thickness of the SHL [t(SHL)] and the E_S peak of each ion-implanted photoresist. The hardness of the SHL of the photoresists increased with increasing ion-implantation doses. This is because the energy, which likely induces hardening of the photoresists supplied from implanted ions to photoresists, increases with increasing the dose. Therefore, the removal rate of the photoresists (v_{rmv}) and the SHL [v_{rmv}(SHL)] decreased with increasing implantation dose. t(SHL) decreased in the order of B → P → As. This is because a heavier ion probably concentrates on the surface more than a lighter ion. Accordingly, v_{rmv} increased in that order. The tendency of t(SHL) listed in Table V was almost the same as that in Table IV, although each absolute value of the thickness indicated in Table V was about half of that in Table IV. Nanoindentation, which is one of the techniques for measurement of hardness using an indenter, may cause twice the difference in the thickness because the SHL, which is hard but brittle, is likely cracked when the indenter reaches the depth of about half of the layer thickness. However, As-ion-implanted photoresists started to harden when ion-implantation doses exceeded 5×10^{13} atoms/cm^2, although B- and P-ion-implanted photoresists started to harden when ion-implantation doses exceeded 5×10^{14} atoms/cm^2. As ions harden photoresists at a lesser dose than B and P ions because a heavier ion may intensively influence the surface more than a lighter ion. However, for the photoresists with a dose of 5×10^{15} atoms/cm^2, the results indicated that the SHL in B- and P-ion-implanted photoresists was harder than that in the As-ion-implanted photoresist. In nanoindentation, the hardness of the SHL in the As-ion-implanted photoresist may be estimated to be lower than the real hardness because the layer is likely very hard but brittle and thin. In other words, the E_S of the SHL may be measured low because the thin layer with much hardening is likely brittle. Results also indicated differences in the hardness and thickness of the SHL attributable to the ion species, as indicated in Table V. The differences may be caused by the distribution of the ions and the energy supplied from the ions to the photoresist, so next, we simulate the behavior of each ion in the photoresist by using SRIM.

Hardening mechanism for an ion-implanted photoresist.— To investigate the differences in the thickness and hardness of the SHL in the ion-implanted photoresists attributable to the ion species, we calculated the distributions of ions implanted into the photoresist and the energy supplied from the ions to electrons and to elements such as C, O, and H, which are components of the photoresist, using SRIM.

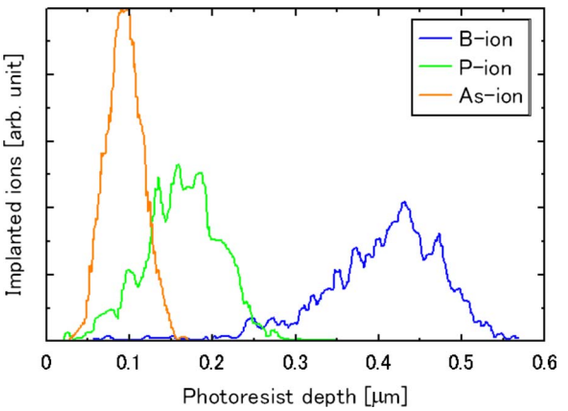

Figure 9. (Color online) Distributions of B, P, and As ions implanted into photoresist calculated by SRIM. The ion acceleration energy was 70 keV.

Figure 9 plots the distribution of each ion implanted into the photoresists, as calculated by SRIM. B-ions were widely distributed to deeper regions in the photoresist. In contrast, As ions were distributed near the surface. The ion distributions concentrated toward the surface in the order of B → P → As. The heavier ions were distributed more toward the surface than the lighter ions. From the results of nanoindentation as indicated in Fig. 6-8, the SHL also shifted toward the surface in the order of B → P → As. The SHL was formed on the subsurface layer through which the ions passed and in which the energy was supplied from ions to photoresists in the interaction between the ions and the photoresists. Therefore, the distributions of ions implanted into a photoresist presumably indicated the similar tendencies of the t(SHL) in each ion-implanted photoresist. However, the ions calculated by SRIM were distributed into deeper regions than the SHL as indicated in Tables IV and V. One reason for this is that the nuclear stopping power of PMMA is low in the SRIM simulation because PMMA without a benzene ring is lower in carbon content than the novolak photoresist with its benzene ring. The second reason is that the ions gradually find it difficult to penetrate deep into the photoresist because the SHL is progressively formed on the photoresist surface during ion implantation. A final reason is that the SHL is sputtered by implanted ions because the film thickness decreased with increases in the dose, as seen in Table I. Here, we consider that the hardening of the photoresist is likely induced by the energy supplied from ions to photoresists based on nuclear and electronic stopping power in interactions between photoresists and ions. The photoresists may carbonize and cross-link among novolak resins by the coupling of radicals that are produced by the dissociation of bonds with low bond energy (e.g., C–O, O–H, and C–H) in the resin due to this energy. Next, we calculate the energy transferred from ions to photoresists.

Figure 10 depicts the distributions of the nuclear and electronic energies (E_N and E_e) supplied from each implanted ion to a photoresist (PMMA). E_N is the nuclear collision energy supplied from each ion to elements (e.g., C, O, and H) in the photoresist, which is an indicator of the damage to the photoresist. E_e is the electron excitation energy supplied from each ion to the electrons in the photoresist, which contributes to forming new bonds by ionization and radical production in the photoresist. The heavier ions concentrated on the surface more than the lighter ions, and the nuclear energy from the heavier ions was greater than the electronic energy they supply. The total energy yield supplied to the photoresists by ion implantation should increase with increasing dose. For that reason, as indicated in Fig. 6-8, photoresists with higher doses hard-

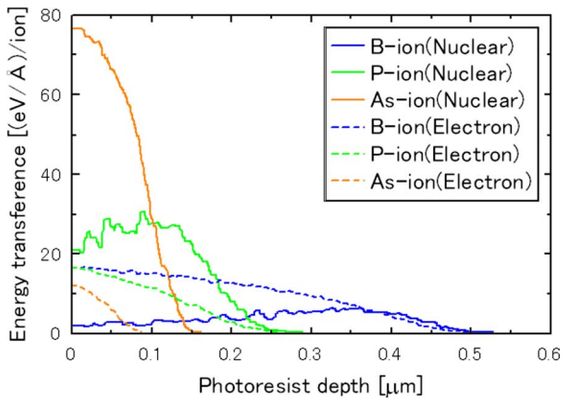

Figure 10. (Color online) Distributions of the nuclear and electronic energies from implanted B, P, and As ions into photoresist, as calculated by SRIM. The ion acceleration energy was 70 keV.

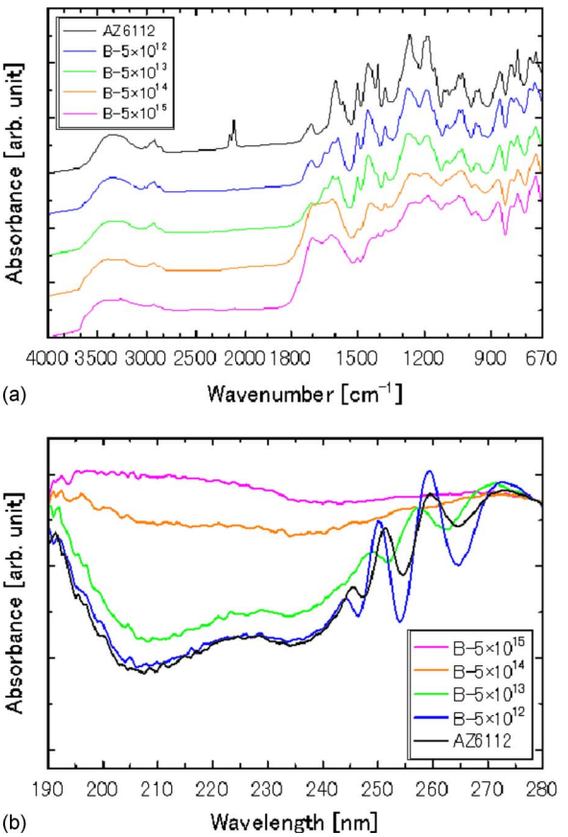

Figure 11. (Color online) Dependencies of (a) FTIR and (b) UV spectra for ion-implanted photoresist on various B-ion-implantation doses. The B-ion-implantation doses were 5×10^{12}–5×10^{15} atoms/cm^2, and the B-ion acceleration energy was 70 keV.

ened more. Table VI lists the E_N, E_e, energy distribution depth (D), and energy densities (E_N/D and E_e/D) for each ion as calculated by SRIM. Here, E_N, E_e, and energy densities were normalized by that for the B ion. When E_N (E_e) supplied from one B ion to the photoresist was 1 (1), that from one P ion was 2.5 (0.42) and that from one As ion was 3.3 (0.14). Here, we compared the impact of each ion on photoresists using E_N/D and E_e/D because D was different for each ion. D for B, P, and As ions was 0.50, 0.25, and 0.08 μm, respectively. When E_N/D (E_e/D) for one B ion was 1 (1), that for one P ion was 5 (0.8) and that for one As ion was 21 (0.9). E_N/D for the heavier ion was greater than that for the lighter ion, so the heavier ion should easily damage the photoresist. In contrast, E_e/D for each ion was nearly similar, so the new bonds should be equally formed regardless of ion species. The new bonds may be easily formed where more interatomic bonds were broken by the implanted ion. For that reason, we deduce that As-ion-implanted photoresists start to harden when the doses exceed 5×10^{13} atoms/cm^2, whereas B- and P-ion-implanted photoresists start to harden when the doses exceed 5×10^{14} atoms/cm^2. Next, to discuss the hardening mechanism for ion-implanted photoresists, we investigate their composition using spectroscopic analysis methods (e.g., FTIR, Raman, UV, and XPS).

Figure 11 depicts the (a) FTIR and (b) UV spectra of the B-ion-implanted photoresist with various ion-implantation doses. The FTIR spectra indicated that the absorption assigned to the OH stretching vibration (around 3400 cm^{-1}), CH stretching vibration (around 2900 cm^{-1}), and CH in-plane deformation vibrations (1400–1500 cm^{-1}) decreased, and the absorption assigned to the C=C stretching vibration (1600–1700 cm^{-1}) increased with increasing implantation doses. The decrease in the OH group's absorption was relatively small. No increase in the absorption of C–O–C (1100–1250 cm^{-1}) with increases in the implantation dose was observed. A schematic model of an ion-implanted photoresist consisting of an ion-mediated structure between novolak resins (covalent bonds among ions and resins) was suggested in Ref. 1 and 2. For the chemical structure of B-ion-implanted photoresists, it has been reported that B–O (1300–1500 cm^{-1}) [38,39] and B–C (1100–1200 cm^{-1}) [38,40] are observed with ion implantation at various ion acceleration energies.[41] However, no increase in the absorption of B-mediated substances with increases in the dose was observed in our study. The UV spectra indicated that the absorption assigned to the π–π^* transition over a broad wavelength range (190–280 nm) increased with increasing dose. Therefore, various kinds of π-conjugated systems should be formed in the photoresist by ion implantation.

Figure 12 depicts the (a) FTIR and (b) UV spectra of the P-ion-implanted photoresist with various ion implantation doses. The FTIR spectra indicated that the absorption of OH and CH decreased and the absorption of C=C increased with increasing implantation dose like B-ion-implanted photoresists. The reduction in the OH group's absorption in P-ion-implanted photoresist was greater than that in B-ion-implanted photoresist. No increase in the absorption of C–O–C with increases in the dose was also observed. In addition, no increase in the absorption of P-mediated substances such as P–C (1290–1330 and 1400–1480 cm^{-1}) and P–O (850–1040 and 1160–1260 cm^{-1}) with increases in the dose was observed in our study. The UV spectra indicated that the absorption of the π–π^* transition (190–280 nm) increased with increasing dose as with B-ion-implanted photoresists. However, for B- and P-ion-implanted photoresists with the same dose, the UV absorption of the P-ion-implanted photoresist exceeded that of the B-ion-implanted photoresist. Therefore, various kinds of π-conjugated systems should be formed in the P-ion-implanted photoresist compared with the B-ion-implanted photoresist. The P-ion-implanted photoresist is likely

Table VI. Nuclear energy (E_N), the electronic energy (E_e), energy distribution depth (D), and energy densities (E_N/D and E_e/D) for each ion as calculated by SRIM. E_N, E_e, E_N/D, and E_e/D for each ion were normalized by that for B ion.

Ion species	E_N (arb. unit)	E_e (arb. unit)	D (μm)	E_N/D (arb. unit)	E_e/D (arb. unit)
B	1	1	0.50	1	1
P	2.5	0.42	0.25	5	0.8
As	3.3	0.14	0.08	21	0.9

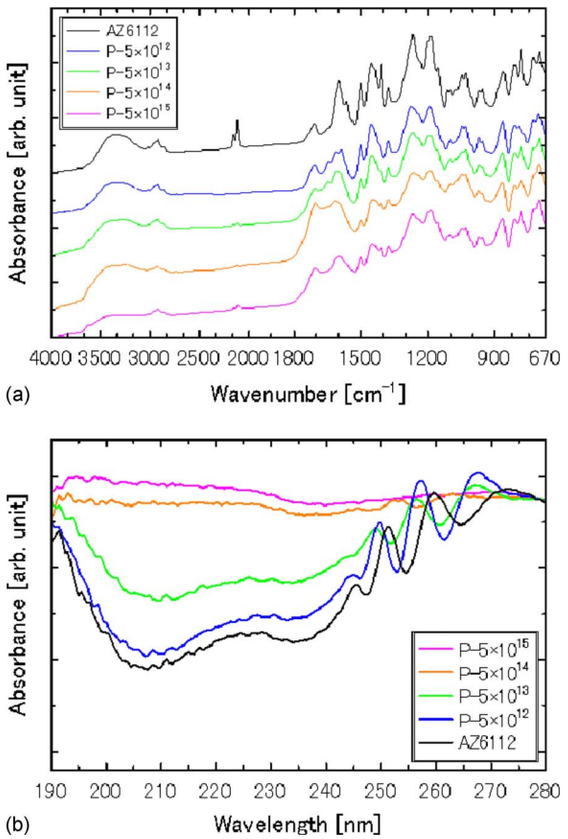

Figure 12. (Color online) Dependencies of (a) FTIR and (b) UV spectra of ion-implanted photoresist on various P-ion-implantation doses. The P-ion-implantation doses were 5×10^{12}–5×10^{15} atoms/cm^2, and the P-ion acceleration energy was 70 keV.

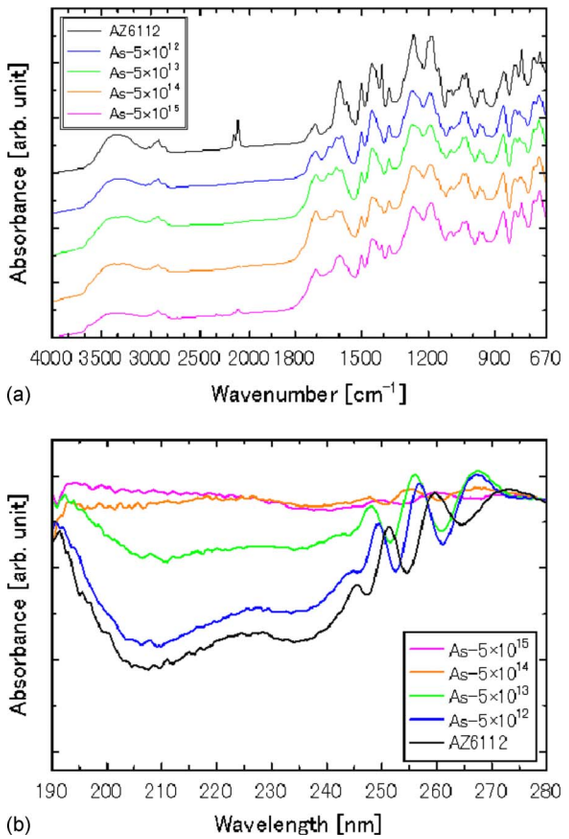

Figure 13. (Color online) Dependencies of (a) FTIR and (b) UV spectra of ion-implanted photoresist on As-ion-implantation doses. The As-ion-implantation doses were 5×10^{12}–5×10^{15} atoms/cm^2, and the As-ion acceleration energy was 70 keV.

more denaturalized than the B-ion-implanted photoresist because the energy supplied from P ions concentrated on the surface more than that from B ions (Fig. 10).

Figure 13 depicts the (a) FTIR and (b) UV spectra of the As-ion-implanted photoresist with various ion-implantation doses. The FTIR spectra indicated that the absorption of OH and CH decreased, and the absorption of C=C increased with increasing implantation dose like B- and P-ion-implanted photoresists. In addition, the reduction in the OH group's absorption in the As-ion-implanted photoresist is greater than that in the B-ion-implanted photoresist as with P-ion-implanted photoresists. No increase in the absorption of C–O–C with increases in the dose was observed. In addition, no increase in the absorption of As-mediated substances such as As–O (around 500 and 800–900 cm^{-1}) or As–C (600–700 and 800–1000 cm^{-1}) with increases in the dose was observed in our study. The UV spectra of As-ion-implanted photoresists indicated the same tendency as those of B- and P-ion-implanted photoresists. However, for P- and As-ion-implanted photoresists with the same dose, the π–π^* transition absorption (190–280 nm) of the As-ion-implanted photoresist exceeded that of the P-ion-implanted photoresist. Therefore, more kinds of π-conjugated systems should be formed in the As-ion-implanted photoresist than in the P-ion-implanted photoresist. The As-ion-implanted photoresist is likely more denaturalized than the P-ion-implanted photoresist because the energy supplied from As ions concentrated on the surface more than that from P ions (Fig. 10).

Figure 14 plots the Raman spectra of B-, P-, and As-ion-implanted photoresists with a dose of 5×10^{14} atoms/cm^2. Absorption at 970 cm^{-1} denoted absorption assigned to the Si wafer substrate. The Raman spectra indicated that the D band at around 1390 cm^{-1} and the G band at around 1580 cm^{-1} increased in the order of B → P → As. The heavier ions would promote more carbonization and cross-linkage of photoresists than the lighter ions. For that reason, we deduce that P- and As-ion-implanted photoresists with a dose of 5×10^{14} atoms/cm^2 would be harder than the B-ion-implanted photoresist with the same dose. Additionally, the reason that the As-ion-implanted photoresist started to harden when the dose exceeded 5×10^{13} atoms/cm^2 whereas the B- and P-ion-

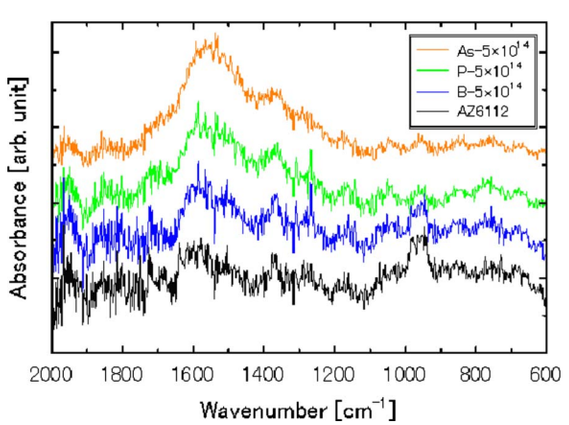

Figure 14. (Color online) Raman spectra of B-, P-, and As-ion-implanted photoresist with a dose of 5×10^{14} atoms/cm^2. The ion acceleration energy was 70 keV.

implanted photoresists started to harden when the dose exceeded 5×10^{14} atoms/cm^2 may be the same as that described above.

We examined the changes in the O and C signals in the XPS spectra of the photoresists by ion implantation. Here, to evaluate each signal from the ion-implanted photoresists, we eliminated background (BG) signals other than peak signals from the XPS data, as indicated in Fig. 15, because no signals associated with implanted ions were observed. Figures 16-18 depict the BG-eliminated XPS spectra of B-, P-, and As-ion-implanted photoresists with various ion-implantation doses. For B-ion-implanted photoresists, the C 1s signal tended to increase with increasing doses, although the O 1s signal was nearly constant regardless of dose. Therefore, B-ion-implanted photoresists would harden by carbonization and the cross-linkage associated with an increase in carbon bonds. However, for P- and As-ion-implanted photoresists, we observed not only an increase in the C 1s signal but also a decrease in the O 1s signal with increasing doses, unlike the B-ion-implanted photoresists. The O 1s signal significantly decreased when the dose exceeded 5×10^{14} atoms/cm^2. The same tendencies were also observed in the OH group's absorption, as indicated in Fig. 12 and 13. The energy supplied from the P and As ions to the photoresists concentrated on the surface more than that from the B ions, and the nuclear energy from the P and As ions was greater than their electronic energy, as indicated in Fig. 10. Besides, E_N/D, which was an indicator of the damage to the photoresist, also increased in the order of B → P → As, although E_e/D, which contributed to forming new bonds, was nearly similar for each ion. Accordingly, for P- and As-ion-implanted photoresists, desorption of OH groups with a relatively low bond energy in novolak resin would be induced by ion implantation because the heavier ion easily breaks chemical bonds in the photoresist. With a desorption of OH groups, we could observe a decrease in the O 1s signal in the XPS spectra. Therefore, P- and As-ion-implanted photoresists would harden by the carbonization and the cross-linkage associated with a decrease in O and an increase in carbon bonds.

Consequently, the hardening of the photoresist should be induced by denaturalization with the energy supplied by the interaction between the ions and the photoresists. For the lighter implanted ions, the ions and the energy were widely distributed to deeper regions in the photoresist, and the nuclear energy was less than the electronic energy. For that reason, a thicker SHL was formed, but its hardening was difficult to promote because the energy density was relatively low. For the heavier implanted ions, the ions and the energy concentrated on the surface, and the nuclear energy was greater than the electronic energy. For that reason, a thinner SHL was formed, but hardening was promoted because the energy density was relatively great. However, the Young's modulus of the SHL in the As-ion-implanted photoresist may be estimated to be lower than the real hardness because the layer is likely very hard but brittle and thin. The nuclear energy relates to damage to the photoresist due to the nuclear collision between ions and the elements that are components of the photoresist, and the electronic energy relates to forming new bonds due to ionization and radical production in the photoresist. E_N/D increased in the order of B → P → As, although E_e/D was nearly similar for each ion. Hence, the impact of ion implantation on the composition of the photoresist should differ between B ions and P and As ions. We suggest that the change in the composition of

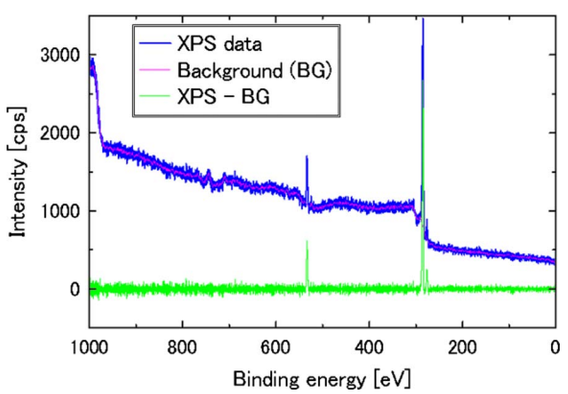

Figure 15. (Color online) XPS wide-scan spectra of nonimplanted photoresist (AZ6112) after eliminating the BG signal of the spectra.

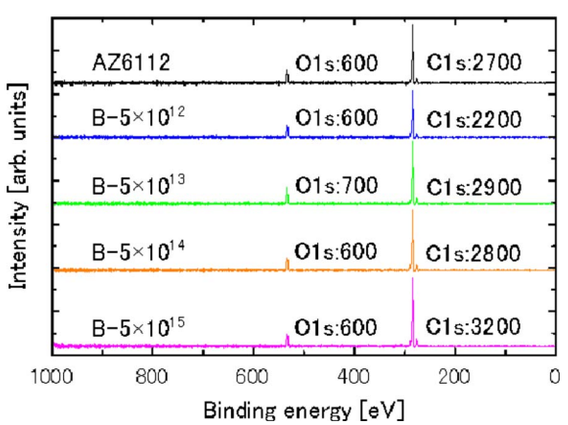

Figure 16. (Color online) BG-eliminated XPS spectra of B-ion-implanted photoresists. The B-ion-implantation doses were 5×10^{12}–5×10^{15} atoms/cm^2, and the B-ion acceleration energy was 70 keV.

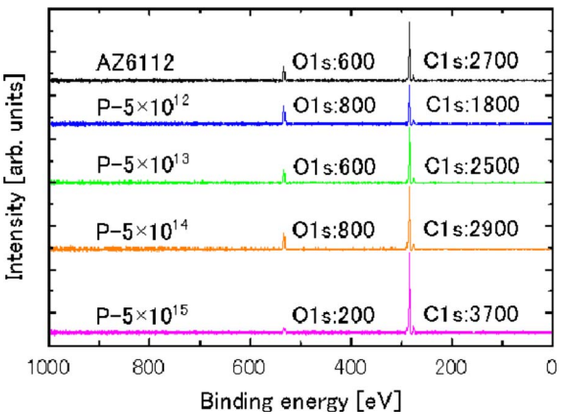

Figure 17. (Color online) BG-eliminated XPS spectra of P-ion-implanted photoresists. The P-ion-implantation doses were 5×10^{12}–5×10^{15} atoms/cm^2, and the P-ion acceleration energy was 70 keV.

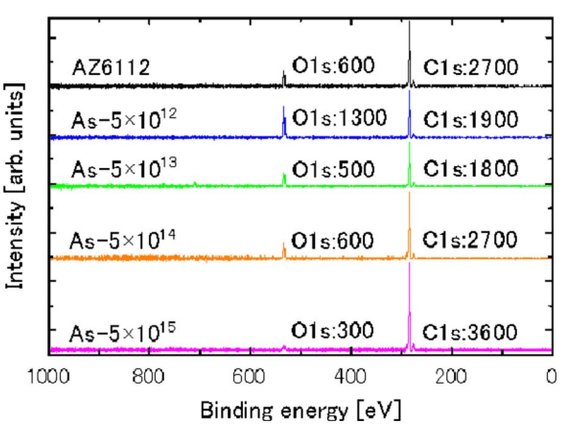

Figure 18. (Color online) BG-eliminated XPS spectra of As-ion-implanted photoresists. The As-ion-implantation doses were 5×10^{12}–5×10^{15} atoms/cm^2, and the As-ion acceleration energy was 70 keV.

B-ion-implanted photoresists is due to carbonization and cross-linkage attributable to the nearly unchanged OH and O 1s, the decrease in CH, and the increase in C=C, C 1s, and π-conjugated systems, whereas that of P- and As-ion-implanted photoresists is due to carbonization and cross-linkage attributable to the decrease of OH, CH, and O 1s and the increase in C=C, C 1s, and π-conjugated systems. We deduce that P and As ions would promote carbonization and cross-linkage of photoresist surfaces more than B ions would. Therefore, we conclude that the photoresists likely carbonize and cross-link between novolak resins by the coupling of radicals that are produced by the desorption of OH (C–OH) and H (O–H and C–H) in novolak resin, attributable to the energy supplied from implanted ions to photoresists.

Conclusions

We examined the relationship between the removal characteristics of ion-implanted photoresist using atomic hydrogen and the hardness of the photoresist. We also investigated the hardening mechanisms for the photoresists using numerical simulation and spectroscopic analysis methods.

Using atomic hydrogen, we examined the characteristics of the removal of positive-tone novolak photoresists into which B, P, and As ions were implanted with doses of 5×10^{12}–5×10^{15} atoms/cm^2 at an acceleration energy of 70 keV. All of the ion-implanted photoresists with doses up to 5×10^{15} atoms/cm^2 were removed regardless of ion species. It was possible to remove each ion-implanted photoresist with an implantation dose below 5×10^{13} atoms/cm^2 like a nonimplanted photoresist (AZ6112), and the hardnesses of the ion-implanted photoresists were similar to that of AZ6112. The removal rates of the photoresists decreased, and the surface of the photoresists hardened with increasing ion-implantation dose once the doses exceeded 5×10^{14} atoms/cm^2. However, after the SHL was removed, the photoresists were removed like AZ6112. The thickness of the SHL [t(SHL)] decreased in the order of B $\rightarrow$ P $\rightarrow$ As, and the removal rates increased in that order. In the photoresist removal using atomic hydrogen, the removal rate was fast if t(SHL) was thin even if hard, whereas the removal rate was slow if t(SHL) was thick even if more or less soft.

Hardening of ion-implanted photoresists should be induced by the energy supplied from ions to photoresists in the interaction between the ions and the photoresists. For B-ion-implanted photoresists, a thicker SHL was formed because the nuclear energy was less than the electronic energy, and the ions were implanted deeper into the photoresist. For P- and As-ion-implanted photoresists, a thinner SHL was formed because the nuclear energy was greater than the electronic energy and the ions concentrated on the surface. E_N/D, which was an indicator of the damage to the photoresist, increased in the order of B $\rightarrow$ P $\rightarrow$ As, although E_e/D, which contributed to forming new bonds, was nearly similar for each ion. The heavier ions likely denaturalized the photoresist surfaces more than the lighter ions from UV and Raman spectra because the heavier ions were distributed on the surface more than the lighter ions. The change in the composition of the B-ion-implanted photoresists is due to carbonization and cross-linkage attributable to the nearly unchanged OH and O 1s, the decrease in CH, and the increase in C=C, C 1s, and π-conjugated systems, whereas that of P- and As-ion-implanted photoresists is due to carbonization and cross-linkage attributable to the decrease in OH, CH, and O 1s and the increase in C=C, C 1s, and π-conjugated systems.

Acknowledgments

The authors are grateful to Professor Hideki Matsumura of the Japan Advanced Institute of Science and Technology and to Kazuhisa Takao and Satoshi Ohya of Tokyo Ohka Kogyo Co., Ltd. Part of this study was supported by the Industrial Technology Research Grant Program (2004) from the New Energy and Industrial Technology Development Organization (NEDO) of Japan.

Kanazawa Institute of Technology assisted in meeting the publication costs of this article.

References

1. S. Fujimura, J. Konno, K. Hikazutani, and H. Yano, *Jpn. J. Appl. Phys., Part 1*, **28**, 2130 (1989).
2. P. M. Visintin, M. B. Korzenshi, and T. H. Baum, *J. Electrochem. Soc.*, **153**, G591 (2006).
3. K. K. Ong, M. H. Liang, L. H. Chan, and C. P. Soo, *J. Vac. Sci. Technol. A*, **17**, 1479 (1999).
4. M. N. Kawaguchi, J. S. Papanu, and E. G. Pavel, *J. Vac. Sci. Technol. B*, **24**, 651 (2006).
5. J. I. McOmber and R. S. Nair, *Nucl. Instrum. Methods Phys. Res. B*, **55**, 281 (1991).
6. Y. Okuyama, T. Hashimoto, and T. Koguchi, *J. Electrochem. Soc.*, **125**, 1293 (1978).
7. J. J. Lee, C. O. Lee, J. Alvis, and S. W. Sun, *J. Electrochem. Soc.*, **135**, 711 (1988).
8. M. N. Kawaguchi, J. S. Papanu, B. Su, M. Castle, and A. Al-Bayati, *J. Vac. Sci. Technol. B*, **24**, 657 (2006).
9. H. Horibe, M. Yamamoto, T. Ichikawa, T. Kamimura, and S. Tagawa, *J. Photopolym. Sci. Technol.*, **20**, 315 (2007).
10. T. Miura, M. Kekura, H. Horibe, and M. Yamamoto, *J. Photopolym. Sci. Technol.*, **21**, 311 (2008).
11. T. Maruoka, Y. Goto, M. Yamamoto, H. Horibe, E. Kusano, K. Takao, and S. Tagawa, *J. Photopolym. Sci. Technol.*, **22**, 325 (2009).
12. M. Yamamoto, Y. Goto, T. Maruoka, H. Horibe, T. Miura, E. Kusano, and S. Tagawa, *J. Electrochem. Soc.*, **156**, H505 (2009).
13. J. N. Smith, Jr. and W. L. Fite, *J. Chem. Phys.*, **37**, 898 (1962).
14. T. W. Hickmott, *J. Chem. Phys.*, **32**, 810 (1960).
15. K. Hashimoto, A. Masuda, H. Matsumura, T. Ishibashi, and K. Takao, *Thin Solid Films*, **501**, 326 (2006).
16. M. Takata, K. Ogushi, Y. Yuba, Y. Akasaka, K. Tomioka, E. Soda, and N. Kobayashi, *Thin Solid Films*, **516**, 847 (2008).
17. H. Horibe, M. Yamamoto, E. Kusano, T. Ichikawa, and S. Tagawa, *J. Photopolym. Sci. Technol.*, **21**, 293 (2008).
18. M. Yamamoto, H. Horibe, H. Umemoto, K. Takao, E. Kusano, M. Kase, and S. Tagawa, *Jpn. J. Appl. Phys., Part 1*, **48**, 026503 (2009).
19. A. Izumi and H. Matsumura, *Jpn. J. Appl. Phys., Part 1*, **41**, 4639 (2002).
20. J. I. Pankove and N. M. Johnson, *Hydrogen in Semiconductors*, Vol. 34, Academic, San Diego (1991).
21. R. Z. Bachrach and R. D. Bringans, *J. Vac. Sci. Technol. B*, **1**, 142 (1983).
22. A. Heya, A. Masuda, and H. Matsumura, *Appl. Phys. Lett.*, **74**, 2143 (1999).
23. T. Sugaya and M. Kawabe, *Jpn. J. Appl. Phys., Part 2*, **30**, L402 (1991).
24. K. Uchida, A. Izumi, and H. Matsumura, *Thin Solid Films*, **395**, 75 (2001).
25. H. Oizumi, A. Izumi, K. Motai, I. Nishiyama, and A. Namiki, *Jpn. J. Appl. Phys., Part 2*, **46**, L633 (2007).
26. W. C. Oliver and G. M. Pharr, *J. Mater. Res.*, **7**, 1564 (1992).
27. M. Lichinchi, C. Lenardi, J. Haupt, and R. Vitali, *Thin Solid Films*, **312**, 240 (1998).
28. X. Chen and J. J. Vlassaka, *J. Mater. Res.*, **16**, 2974 (2001).
29. B. D. Beake, G. J. Leggett, and M. R. Alexander, *J. Mater. Sci.*, **37**, 4919 (2002).
30. G. M. Pharr, W. C. Oliver, and F. R. Brotzen, *J. Mater. Res.*, **7**, 613 (1992).
31. J. F. Ziegler, J. P. Biersack, and M. D. Ziegler, *SRIM "The Stopping and Range of Ions in Matter,"* Lulu, Morrisville, NC (2008) (http://www.srim.org).
32. T. C. Smith, in *Handbook of Ion Implantation Technology*, J. F. Ziegler, Editor, Elsevier Science, New York (1992).
33. H. Umemoto, K. Ohara, D. Morita, T. Morimoto, M. Yamawaki, A. Masuda, and H. Matsumura, *Jpn. J. Appl. Phys., Part 1*, **42**, 5315 (2003).
34. H. Umemoto, K. Ohara, D. Morita, Y. Nozaki, A. Masuda, and H. Matsumura, *J. Appl. Phys.*, **91**, 1650 (2002).
35. T. Ishibashi, S. Shimoda, T. Furukawa, I. Nitta, and H. Yoshida, *Trans. Jpn. Soc. Mech. Eng.*, **53**, 2193 (2007).
36. J. Xu, J. Y. Rho, S. R. Mishra, and Z. Fan, *J. Biomed. Mater. Res. Part A*, **67A**, 719 (2003).
37. G. M. Pharr, W. C. Oliver, and F. R. Brotzen, *Mater. Sci. Eng., A*, **445–446**, 323 (2007).
38. Y. J. Zou, X. W. Zhang, Y. L. Li, B. Wang, H. Yan, J. Z. Cui, L. M. Liu, and D. A. Da, *J. Mater. Sci.*, **37**, 1043 (2002).
39. G. D. Sorarù, N. Dallabona, C. Gervais, and F. Babonneau, *Chem. Mater.*, **11**, 910 (1999).
40. A. Annen, M. Sass, R. Beckmann, A. Von Keudell, and W. Jacob, *Thin Solid Films*, **312**, 147 (1998).
41. N. Nagai, T. Imai, K. Terada, H. Seki, H. Okumura, H. Fujino, T. Yamamoto, I. Nishiyama, and A. Hatta, *Surf. Interface Anal.*, **33**, 545 (2002).